metals

MDPI

Article

Wear and Corrosion Resistance of CrYN Coating in Artificial Seawater

Man Li [1,*], Yunjiang Yu [2], Changwei Zou [3], Canxin Tian [3], Zesong Wang [3] and Yanxiong Xiang [3]

[1] Faculty of Mechanical and Electrical Engineering, Lingnan Normal University, Zhanjiang 524048, China
[2] Faculty of Chemistry and Chemical Engineering, Lingnan Normal University, Zhanjiang 524048, China
[3] Faculty of Physics Science and Technology, Lingnan Normal University, Zhanjiang 524048, China
* Correspondence: oqlm@163.com

Abstract: In this study, CrYN coatings were prepared using multi-arc ion plating at various substrate bias voltages (−50 V, −100 V, −150 V, and −200 V). X-ray diffractometry and scanning electron microscopy were used to characterize the composition and microstructure of the coatings. An electrochemical workstation and a ball-on-disk tribometer were used to investigate their corrosion and friction behavior. The results show that grain refinement can be achieved through the addition of yttrium (Y) and that the surfaces of coatings prepared under different bias voltages have varying smoothness and compactness. It was shown that surfaces prepared under −100 V bias voltages were relatively smooth and dense in structure, corresponding to a Y content of 2.83 at.%; CrYN coatings at −100 V were shown to have the highest corrosion potential and a low self-corrosion current, equating to superior corrosion resistance. Additionally, the friction coefficients of deposited CrYN coatings under bias voltages of −100 V were less than 0.2. Therefore, the coatings under bias voltages of −100 V had the minimum wear rate due to its structure, corrosion resistance, and friction.

Keywords: CrYN coatings; substrate bias voltage; corrosion resistance; mechanism; artificial seawater

Citation: Li, M.; Yu, Y.; Zou, C.; Tian, C.; Wang, Z.; Xiang, Y. Wear and Corrosion Resistance of CrYN Coating in Artificial Seawater. *Metals* **2023**, *13*, 183. https://doi.org/10.3390/met13020183

Academic Editors: Sebastian Feliú, Jr. and Federico R. García-Galván

Received: 7 December 2022
Revised: 9 January 2023
Accepted: 11 January 2023
Published: 17 January 2023

1. Introduction

With the rapid development of marine economies, the need for and production of marine engineering equipment with good anti-corrosion properties and resistance to wear in marine environments has increased [1–3]. Usually, the key metal and alloy components (e.g., gears, bearings, and propellers) in engineering equipment are subjected to a seawater environment over a considerable length of time. This eventually compromises the equipment's safety and impacts the equipment's lifetime, leading to its eventual failure due to the synergistic effect of friction and corrosion [4]. Adhering protective coatings to the surfaces of marine materials using different deposition processes improves the wear and corrosion resistance properties of the materials [5]. Among the many coating processes used, multi-arc ion plating is prominent in the preparation of surface coatings for key marine equipment components, such as metal fasteners and connections, because of its high dissociation rate and deposition rate. A systematic study regarding the friction and corrosion behaviors of such coatings in a corrosive marine environment would provide an experimental and theoretical basis for the application of coated engineering equipment in such extreme conditions.

CrN coatings are widely used on the surfaces of marine equipment components due to their good anti-oxidation, anti-corrosion, and wear-resistance properties [6–8]. However, the tiny gaps in a CrN coating with a columnar crystal structure provide direct-access channels for Cl^- ions, causing the matrix to suffer from corrosion [9,10]. At present, research regarding the enhancement of the anti-friction and anti-corrosion properties of CrN coatings is divided into two main areas. One involves a multi-layer or gradient-layer structural design for a coating to improve the bonding force between it and the substrate, to improve its interfacial toughness and anti-crack propagation ability, and to realize the composite functions

that each layer has [11–15]. Designing CrN/Cr multi-layers with composition or thickness modulation, for example, maintains the high-hardness characteristics of the coating while reducing its brittleness and internal stress; this also improves its mechanical, anti-corrosion, and tribological properties [16,17]. The second area of research involves the construction of a ternary- or multiple-alloy coating by adding elements, such as a metal (e.g., Ti, Al, Zr, Y [18–22]) or a nonmetal (e.g., Si, C, B [23–26]) to a traditional binary CrN coating to improve its physical and mechanical properties. In a metallurgical context, Radu et al. [27] reported that alloy grains could be refined by doping them with a small amount of rare-earth Y. Wu et al. [28] found that, after adding a Y element into a CrN coating, the Y ion replaced the Cr ion to form a CrYN solid solution due to the solid solution mechanism, the hardness increased from 12. 9 to 13.7 GPa, and the coating adhesion was increased. Rovere et al. [29] found that, after adding a Y element into a CrAlN coating, the column length of the crystal columnar structure became shorter, and the hardness increased from 31.4 to 38.1 GPa due to the solid solution mechanism forming a CrAlYN solid solution. Wang et al. [30] found that, when the Y content was lower than 2.67 at%, the coating was preferentially oriented to (111), the surface morphology changed from granular to polygonal, crystals were refined, and the compactness was enhanced. With a Y content of 1.13 at%, the Young's modulus and hardness maximum values were 390.6 and 29.4 GPa, respectively. The best corrosion performance was obtained with a Y content of 1.98 at%, wherein the corrosion current and corrosion potential were 3.564×10^{-6} A cm^{-2} and −0.4461 V.

Y-nitride-containing coatings, in terms of wear and corrosion resistance, show good performance; however, their wear and corrosion resistance properties in seawater environments have not been systematically studied. Therefore, in this paper, CrYN coatings were prepared using multi-arc ion plating to study their friction and corrosion behaviors in artificial seawater and provide theoretical support for the application of this type of coating in marine environments.

2. Materials and Methods

2.1. Coating Deposition

CrYN coatings under various substrate bias voltages (−50 V, −100 V, −150 V, and −200 V) were deposited on a 316 stainless steel substrate (20 mm × 20 mm × 3 mm) and the surface of single-crystal silicon (111) using multi-arc ion plating. Ar (99.99 at.%) was used as the working gas, and N_2 (99.99 at.%) was used as the reaction gas. An alloy target (with a purity of 99.9% CrY, Cr:Y = 95:5 at.%) and a pure Cr target (with a purity of 99.9%) were selected as cathode targets. The deposition system structure is shown schematically in Figure 1, and detailed preparation parameters are shown in Table 1.

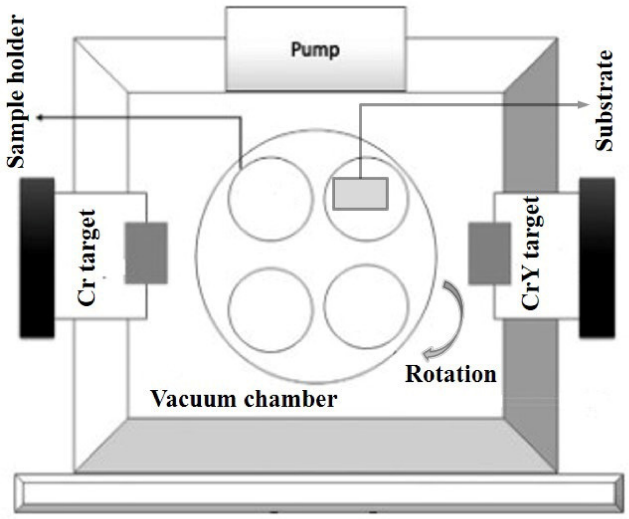

Figure 1. Schematic diagram of arc-deposited CrYN coatings.

Table 1. Preparation parameters of CrYN coatings.

Bias Voltage/V	Transition Layer CrN/Cr			CrYN		
	Current/A	Pressure/Pa	Time/min	Current/A	Pressure/Pa	Time/min
−50, −100, −150, −200	80	2.0	10	70	1.0	120

2.2. Characterization of Coating

Field emission scanning electron microscopy (SEM, JSM-7610F, Tokyo, Japan) was used to observe the surface and wear scar morphologies of the CrYN coatings, X-ray diffraction (XRD, MiniFlex II, Rigaku, Japan) was used to investigate the structure of the coatings, and energy dispersive spectroscopy (EDS, NORAN System 7, Waltham, MA, USA) was used to analyze their chemical components. The coefficient of the friction of the coatings was determined using a tribometer (CFT-1, Zhongkekaihua Inc., China). A GCr15 ball with a diameter of 4 mm was used as the rubbing material, the GCr15 hardness was 850 HV, the abrasive diameter was 4 mm, the rotation speed was 0.1 m/s, the load was 5 N, and the sliding time was 3600 s. After being tested, the friction morphology of the coating surface was observed using an Optical Profiler (Bruker Countor GT K 3D, Billerica, MA, USA), and the wear rate of the coating wear scars was calculated using Equation (1):

$$w_{s,b} = \frac{2\pi\pi r}{FL} \quad (1)$$

where F is the test load, L is the frictional length, r is the coated wear scar radius, and A is the average wear area of a coating wear scar.

The electrochemical performance in artificial seawater was tested using an electrochemical workstation (Autolab, PGSTAT-100N, EcoCheime, The Netherlands). The electrochemical impedance spectroscopy (EIS) frequency was set to 10 mHz to 100 kHz with a sinusoidal perturbation of 10 mV; potentiodynamic polarization curves were scanned in the range of −1.0 to 1.0 V at a scan rate of 20 mV/min. To guarantee data stability, the tests were repeated three. The configuration of the artificial seawater complied with the ASTM D1141-98(2021) standard [31], and detailed parameters are shown in Table 2. The corrosion current density, i_{corr}, and corrosion potential, E_{corr}, of the CrYN coatings were calculated via Tafel extrapolation. Polarization resistance was calculated using the Stern–Geary Equation (2) [32]:

$$i_{corr} = \frac{\beta_a \beta_c}{2.303 R_p (\beta_\alpha + \beta_c)} \quad (2)$$

where β_a is the Tafel anodic polarization slope and β_c is the Tafel cathodic polarization slope.

Table 2. Chemical composition of artificial seawater.

Component	NaCl	KCl	Na_2SO_4	$NaHCO_3$	$MgCl_2$	KBr	$CaCl_2$	H_3BO_3	$SrCl_2$	NaF
Concentration (g/L)	24.530	0.695	4.090	0.201	5.200	0.101	1.160	0.027	0.025	0.003

3. Results and Discussion

3.1. Coating Structure, Morphology and Mechanical Properties

The chemical components of the deposited CrYN coatings under different substrate bias voltages are listed in Table 3. The atomic concentration ratio (Cr/Y) range was from 21.8.1 to 26.3, which was higher than that of the CrY cathode target. This indicated that the arc-current of 70 A used in the preparation process of the CrYN coatings caused the evaporation rates of Cr and Y atoms to differ. The evaporation rate of Y atoms was lower than that of the Cr atoms at the test temperature designed in this paper. However, the Cr/Y ratio gradually decreased with increasing bias voltage. This indicated that the

bombardment effect of Y ions enhanced with increasing bias voltage, meaning that the concentration of Y atoms in the coating gradually increased from 2.58 at.% to 3.4 at.%.

Table 3. Chemical composition of CrYN coatings.

Sample	Composition/at.%		
	Cr/at.%	Y/at.%	Cr/Y%
CrYN-1	67.85	2.58	26.3
CrYN-2	68.78	2.83	24.3
CrYN-3	71.66	3.1	23.1
CrYN-4	74.16	3.4	21.8

Figure 2a–d show the SEM surface morphologies of the deposited CrYN coatings under different bias voltage conditions. Some particles and holes, with sizes ranging from hundreds of nanometers to several micrometers, existed on the surface of the coating, forming microdroplets, pinholes, and molten pits [33,34]. With increasing substrate bias voltages (−50 V, −100 V, −150 V, and −200 V), the number and diameter of large particles on the surface of the coating decreased, and the number of coating surface defects decreased. These improvements can be explained by the ion bombardment mechanism: as the bias voltage increases, the ion bombardment effect is enhanced, and surface droplets are sputtered off by high-energy ion bombardment. In addition, during arc ion plating, a substrate with negative bias applied to a substrate has a repulsive effect on the negatively charged droplets, and, when the bias is increased, the repulsive effect is enhanced, and the number of droplets reaching the substrate surface is reduced. Figure 2 shows that the surfaces of the CrYN-2, CrYN-3, and CrYN-4 coatings have a larger decrease in defects than those of the CrYN-1 coating.

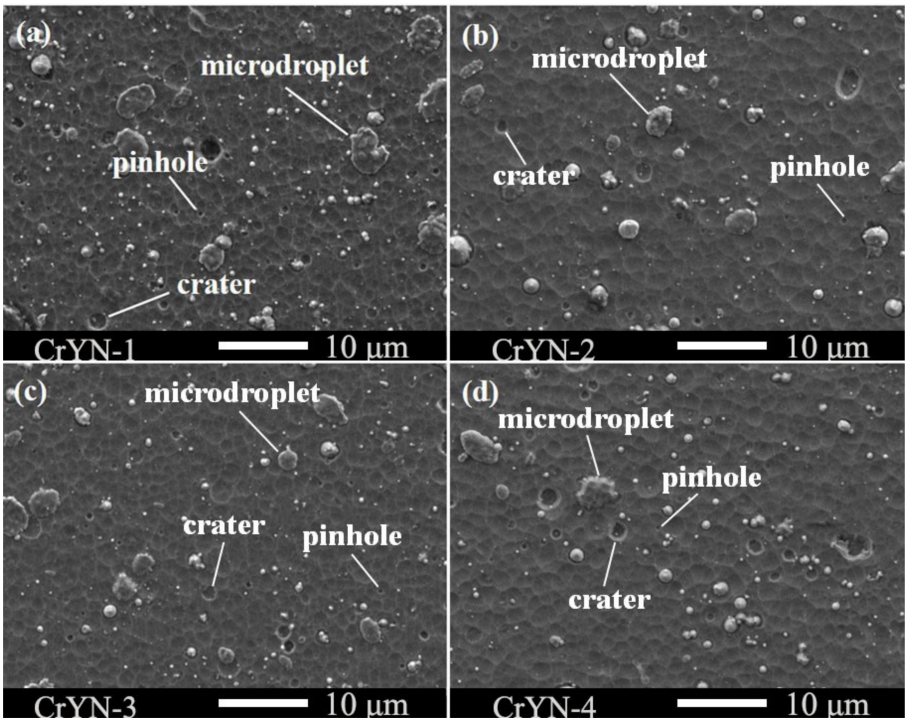

Figure 2. Surface morphologies (**a**–**d**) of CrYN coatings deposited at various substrate bias voltages.

Figure 3a–d show SEM cross-sectional images of the deposited CrYN coatings under different substrate bias voltages. Figure 3a shows that the deposited CrYN-1 coating has a relatively columnar, crystal structure. The large particles on the surface originated from unfused metal droplets in the target, similar to what is observed in Figure 2a. The

compactness of the CrYN-2 coating and the CrYN-3 coating was better than that of the CrYN-1 coating, mainly because, with increasing bias voltage, the bombardment with high-energy ions is enhanced, and the active Y element increases the nucleation rate of film deposition, inhibits grain growth, and thus increases the coating density [35–37]. In addition, in the process of high-energy ion bombardment, atoms can enter the grain gap and form a denser structure [38]. As the bias voltage increased, the thickness of the CrYN coating first increased and then decreased. It is believed that negative bias pressure has two main effects on the deposition rate. One is the accumulation effect, in which the particles evaporated from the target material adhere to the substrate; the other is the resputtering effect on the coating, i.e., the exfoliation of the deposited coating [39]. Variations in coating thickness are related to the sputtering process, the particle accumulation effects produced, and mutual competition for resputtering effects. At the beginning of the sputtering process, the deposition rate gradually increased with the elevation of the matrix bias, although the energy of the bombarded ions also became larger at this time, producing a resputtering effect; however, the accumulation effect was dominant; the number of particles sputtered onto the substrate increased, and the thickness increased. In this study, when the bias voltage was excessive (−200 V), the energy of the deposited ions was too high, and compressive stress created pores in the coating (Figure 3d), reducing the coating's compactness [40]. At this time, the resputtering effect enhanced and the deposition rate decreased.

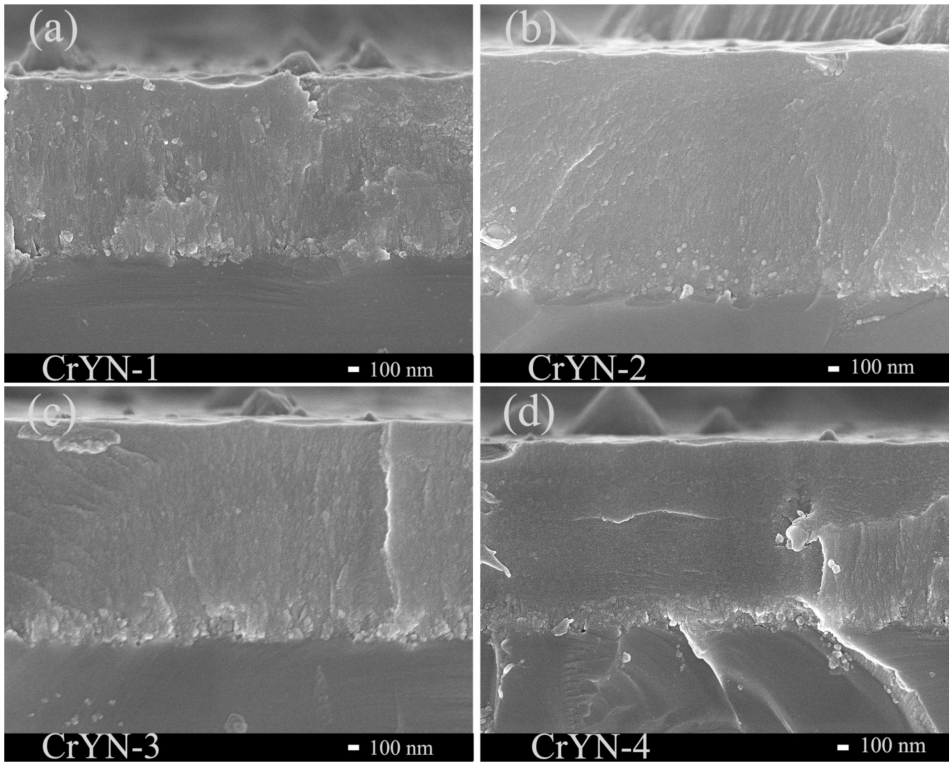

Figure 3. Cross-sectional (**a**–**d**) SEM images of CrYN coatings deposited at various substrate bias voltages.

Figure 4 shows XRD patterns of the deposited CrYN coatings under different bias voltages. Without Y-doping, the diffraction angles (2θ) were 37.49°, 43.59°, and 63.35°, corresponding to a CrN (111), (200), and (220) face-centered cubic structure. The appearance of the α-Cr metallic phase and the hexagonal, closely packed *hcp*-Cr_2N phase near the CrN (200) peak may have been because of excessive Cr in the coating caused by insufficient nitrogen gas during deposition, which is consistent with the results displayed in Table 3. As the substrate bias voltage increased, the CrN (111), (200), and (220) peak intensities decreased and increased in width at half height. This indicates that the enhancement of

plasma energy and surface bombardment would lead to a grain refinement, similar to what is observed in Figure 3 [41].

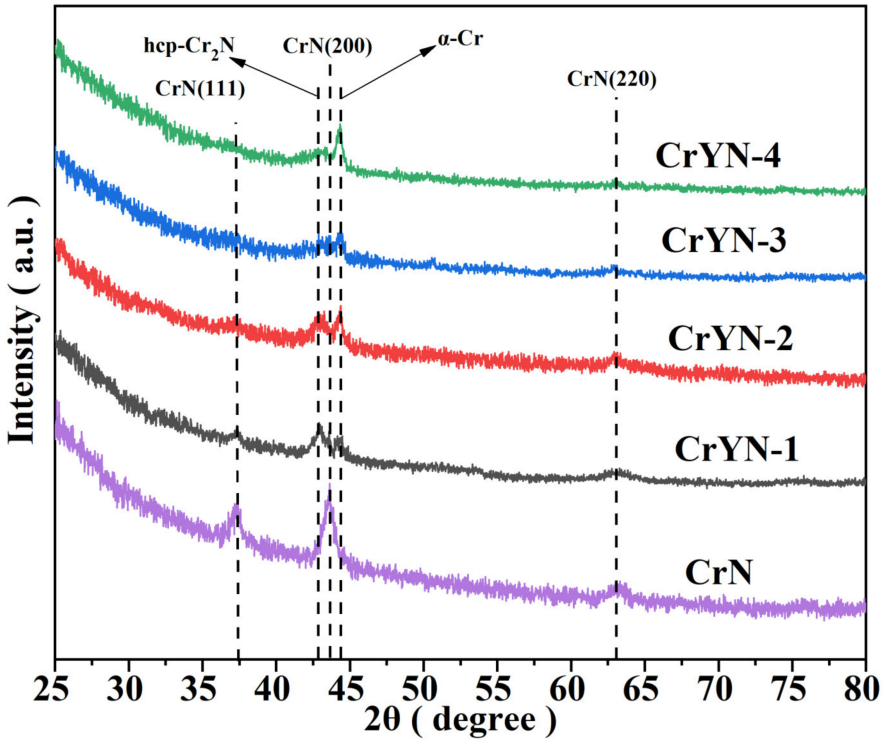

Figure 4. XRD patterns of CrYN coatings deposited at various substrate bias voltages.

Figure 5 shows the hardness of the deposited CrYN coatings under different substrate biases. The substrate bias increased from −50 V to −200 V, and the microhardness increased from 1985 hv to 2192 HV due to the grain refinement and structure densification.

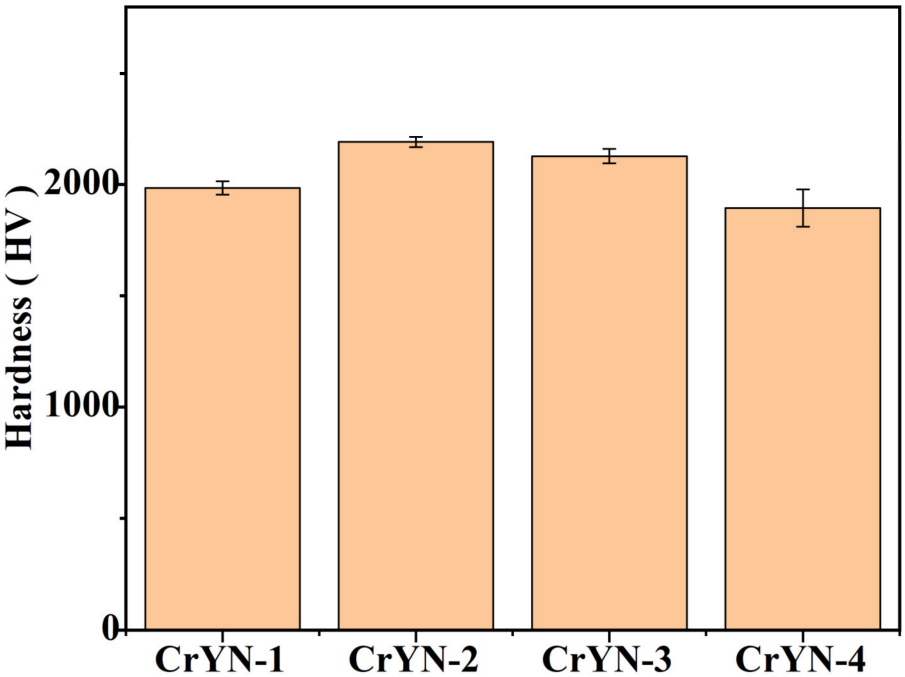

Figure 5. Hardness of CrYN coatings deposited at various substrate bias voltages.

3.2. Corrosion Resistance

Figure 6a shows Nyquist plots of the CrYN coatings. In EIS tests, the radius of the capacitive loop was high and low, and the phase angle was close to the degree of the height number, which is generally used to judge the impedance performance of coatings [42]. The CrYN-2 coating was inside all of the coatings with the highest radius, indicating that it displayed the best corrosion resistance performance. The phase angles of several coatings were relatively close, and that of the CrYN-2 coating was relatively large. This indicates that the CrYN-2 coating could provide better protection against seawater erosion than the CrYN-1 and CrYN-3 coatings.

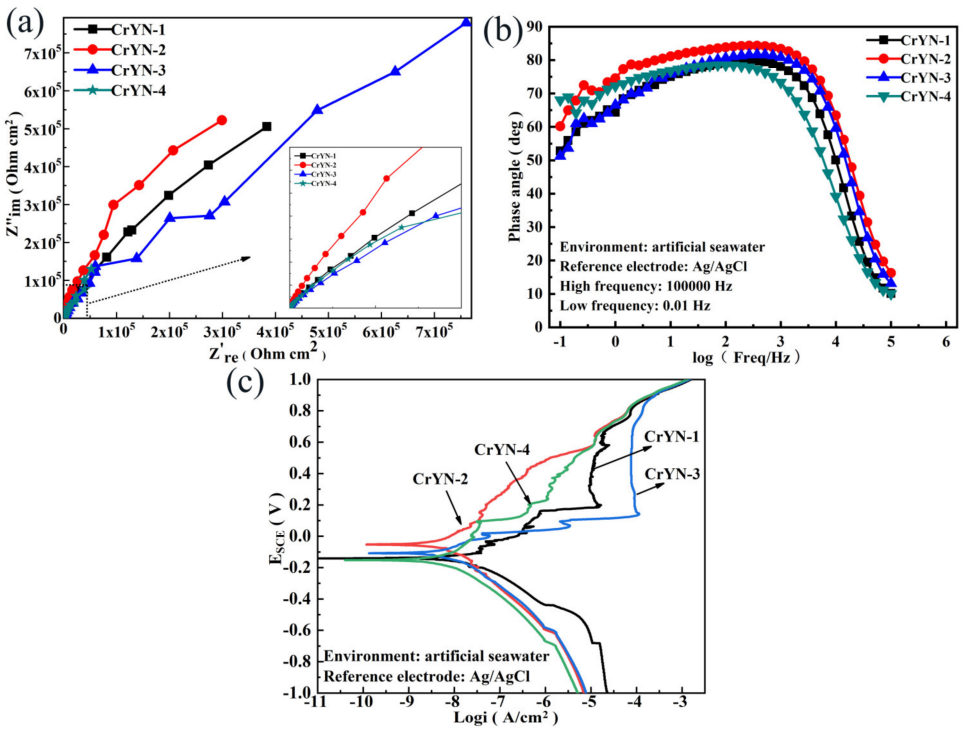

Figure 6. Electrochemical corrosion plots of CrYN coatings deposited at different substrate bias voltages and tested in artificial seawater: (**a**) Nyquist, (**b**) Bode, and (**c**) Tafel.

Figure 6c shows the potentiodynamic polarization curves of the CrYN coatings in artificial seawater. Using Equation (3), the deduced electrochemical corrosion parameters are listed in Table 4. The self-corrosion potential (E_{corr}) of the CrYN-2 coating was an order of magnitude higher than that of the CrYN-3, CrYN-1, and CrYN-4 coatings. The self-corrosion current density (i_{corr}) of the CrYN-2 coating was not much different from that of the CrYN-3 and CrYN-4 coatings but decreased by an order of magnitude relative to the i_{corr} values of the CrYN-1 coating. This shows that the CrYN-2 coating displayed the best corrosion resistance in the potentiodynamic polarization test, followed by the CrYN-3 coating. This is because of the dense and refined grain of the coating, which inhibited the propagation of micro-cracks and vias at the micro-structure level, decreasing the connectivity of pores, and thereby improving the corrosion resistance. Abd et al. found that, in the columnar crystal structure, due to its relatively loose structure, the corrosion solution penetrated relatively easily through the defects to the substrate. The penetration of the corrosion solution can be effectively prevented by strengthening the compactness of the coating [43]. The CrYN-1 coating had lower corrosion potential and the highest corrosion current density due to its loose columnar crystal structure. This structure comprised vertical grain boundaries and pores through the coating, providing highly efficient channels for the rapid diffusion of the corrosive electrolyte to the substrate. In addition, the surface of the CrYN-1 coating had many large particles and defects, such as pinholes. Additionally, ions

in the corrosion medium could easily enter the holes, enhancing the corrosion of the coating. Barshilia et al. found that increasing the coating thickness obviously improved defects such as micro cracks, pinholes, etc., and increased the difficulty with which the corrosion solution entered the substrate [44]. The CrYN-4 coating exhibited the lowest corrosion potential, mainly due to the occurrence of pores in the interior of the coating. The cracks provided channels for the diffusion of the corrosion medium and, in turn, reduced the corrosion resistance of the coating. In the polarization curves, noise fluctuation appeared, indicating vigorous electrochemical corrosion. The possible reasons for this are: there were a large number of particles and holes on the surface of the coating, which collapsed during the polarization curve test, providing highly efficient channels for the rapid diffusion of the corrosive electrolyte, thus causing pitting corrosion and localized corrosion perforation [45].

Table 4. Electrochemical corrosion parameters inferred from Tafel plots in Figure 6c.

Sample	E_{corr} (V)	β_a (V)	β_c (V)	i_{corr} (10^{-6} A/cm^2)	R_p (kΩ·cm^2)
CrYN-1	−0.141 ±0.020	0.134 ±0.022	0.158 ±0.019	17.051 ±2.740	1847 ±211
CrYN-2	−0.052 ±0.010	0.174 ±0.016	0.132 ±0.008	5.803 ±0.194	5620 ±31
CrYN-3	−0.117 ±0.013	0.176 ±0.014	0.073 ±0.003	4.677 ±0.421	4798 ±337
CrYN-4	−0.151 ±0.010	0.158 ±0.009	0.150 ±0.005	4.976 ±0.470	6723 ±526

3.3. Tribological Properties

Figure 7 shows curves of the coefficient of friction (COF) for the CrYN coatings in artificial seawater. The average friction coefficients of the coatings were low, all being less than 0.25. In the process of friction in artificial seawater, artificial seawater plays a lubricating role, thus reducing the friction coefficient. Shan et al. [46] found that, during the friction process, large particulate matter on the surfaces of the coatings forms wear debris at the friction side. After absorbing moisture, the wear debris forms a layer of hydrated transfer film with a low shear strength, which reduces the friction of coatings. Wang et al. [47] found that Ca^{2+} and Mg^{2+} ions in artificial seawater—due to the continuous friction, which makes the local temperature increase—react with water tribochemically. The generation of $CaCO_3$, Mg (OH) $_2$, etc., with a boundary lubricating effect.

The average friction coefficients of the CrYN-4 and CrYN-1 coatings were higher than those of CrYN-2 and CrYN-3 because the CrYN-1 coating comprised a large-grain, columnar crystal structure. Therefore, artificial seawater easily entered between the grain boundaries, destroying the coating and increasing the friction coefficient of the friction interface. Due to the creation of cracks in the CrYN-4 coating, artificial seawater seeped into the coating pores after a period, destroying the coating and increasing the friction coefficient. However, the CrYN-4 coating was denser than the CrYN-1 coating, therefore the rate at which artificial seawater entered into the pores of the CrYN-4 coating was lower, producing a slow rise in the friction coefficient.

The CrYN-2 and CrYN-3 coatings were relatively dense, meaning artificial seawater had difficulty in entering the interior of the coatings. This produced a lubrication effect on the friction interface, resulting in an average friction coefficient as low as 0.20.

The wear scar micro-structure of CrYN/GCr15 subjected to artificial seawater is shown in Figure 8. The inter-grain voids in the interior of the CrYN-1 coating were large, and artificial seawater easily entered into the voids. This weakened the inter-grain bonding, making the CrYN-1 coatings more likely to peel off from the substrate, worsening the wear scars, and making the wear scars form black debris along the sliding direction of the wear track, adhering them to the friction surface. The grains of the CrYN-2 and CrYN-3 coatings were fine, the coatings were dense, and the wear scar surfaces were smooth. The wear scar surfaces had dimples that were produced when the large particles on the coating surface

were pulled out upon a little friction. There were pores in the CrYN-4 coating, and artificial seawater entered the cracks. The coating was then easily peeled off, forming sporadic lamellar debris under the action of contact stress on the wear side of the surface.

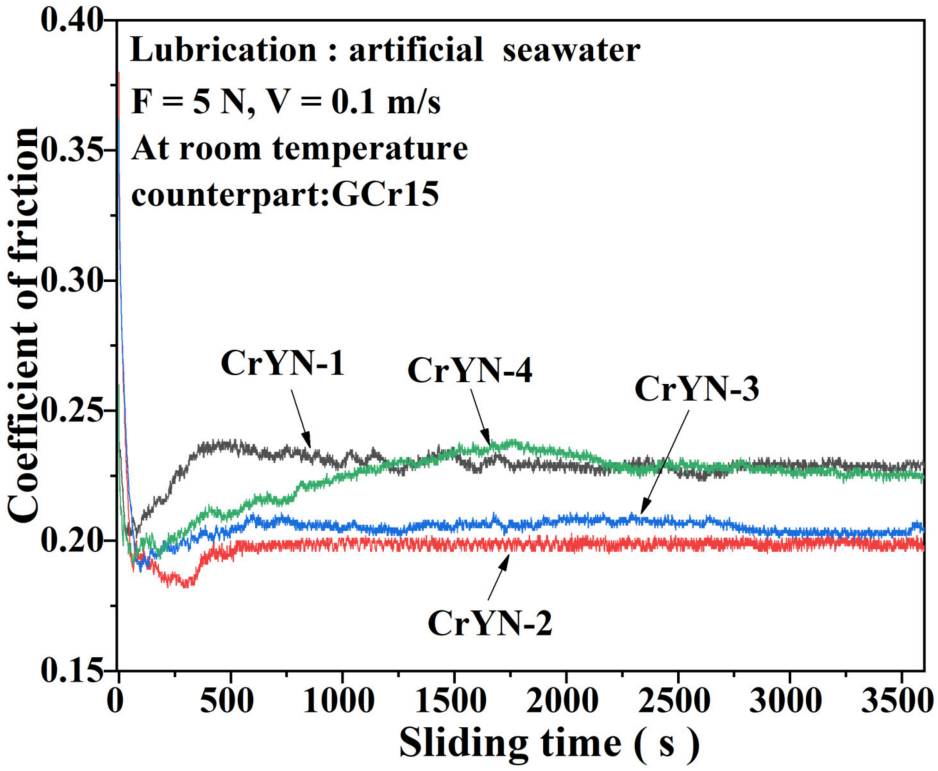

Figure 7. The curves of COF for CrYN-1, CrYN-2, CrYN-3, and CrYN-4 coatings in artificial seawater.

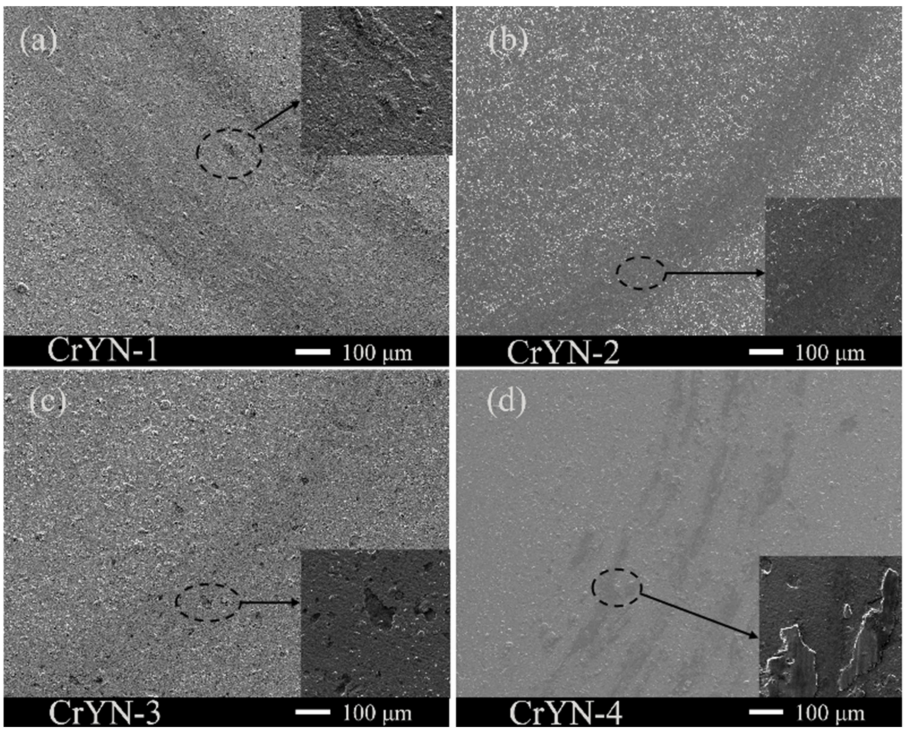

Figure 8. SEM images of Wear track and enlarged on CrYN coating against GCr15 ball in artificial seawater.

The EDS spectrum of the wear scars in Figure 9 shows that, in addition to the components of the coating itself in the artificial seawater, some other elements existed, such as Ca and Mg. These were transferred from the artificial seawater to the coating during the friction process, and species such as $CaCO_3$ and $Mg(OH)_2$, with a good lubrication effect, may have been generated [48]. Some O elements were also deposited, indicating that, during the friction process, the coatings and water underwent a tribochemical reaction [19]. This resulted in the formation of an oxide, and the possible chemical reactions are presented as follows:

$$2CrN + 3H_2O \rightarrow Cr_2O_3 + 2NH_3 \quad (3)$$

$$2Cr_2N + 6H_2O \rightarrow 2Cr_2O_3 + 2NH_3 + 3H_2 \quad (4)$$

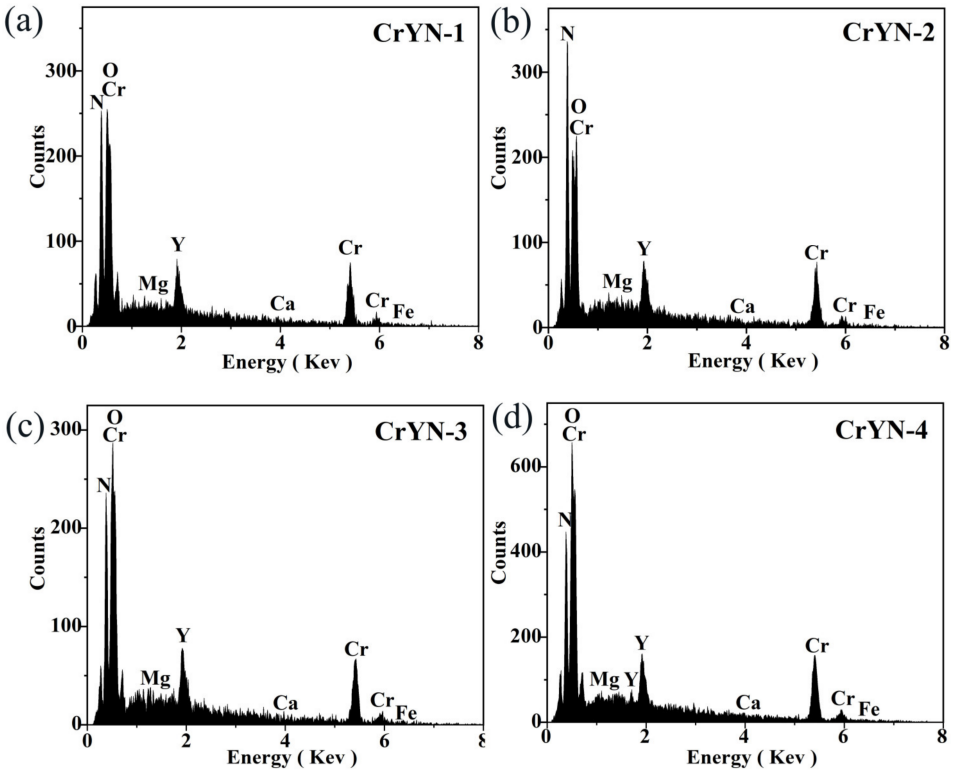

Figure 9. EDS spectrum of sliding wear tracks of GCr15 on CrYN coatings in artificial seawater.

Judging from this analysis, it can be stated that the wear mechanism of the CrYN coating in artificial seawater was a mix of tribochemical wear and adhesive wear, with the tribochemical wear producing the greatest effect.

The wear rates of the deposited CrYN coatings with different substrate bias voltages in artificial seawater are shown in Figure 10. For the same material, when cut through wear, higher surface hardness can effectively block the cutting of wear ball and thus improve the wear resistance performance. As the microhardness of CrYN coating increased, the wear rate became smaller and the wear resistance performance improved. The wear rates of CrYN-1 and CrYN-4 were significantly higher than those of CrYN-2 and CrYN-3. The main reasons for this are as follows: Firstly, as evidenced by the surface morphology of the CrYN-1 coating—which had obvious columnar, crystal characteristics with large grain gaps—during the friction process, a high-pressure injection state was created, which enabled artificial seawater to enter the gaps. This increased the exfoliation of the coating and then increased the wear rate. Secondly, as evidenced by the CrYN-4 coating's cross-sectional morphology, some pores appeared in the coating layers, meaning that the coating particles became easier to peel off upon friction, thereby increasing the wear rate. Thirdly, the analysis showed that the corrosion resistance of the CrYN-1 coating was weaker than that of the CrYN-2 and CrYN-3 coatings; as the weakening effect of seawater on the grain

gaps of the coatings was enhanced, the wear loss increased. In contrast, the CrYN-2 and CrYN-3 coatings had a dense structure, high self-corrosion potential, and small self-corrosion current density, meaning the artificial seawater had difficulty in accessing the interior of these coatings to achieve a lower wear rate. Overall, the wear resistance of the CrYN coating deposited by a bias voltage of −100 V in artificial seawater was shown to be the best. The CrYN coating layers deposited at −150 V were the second best.

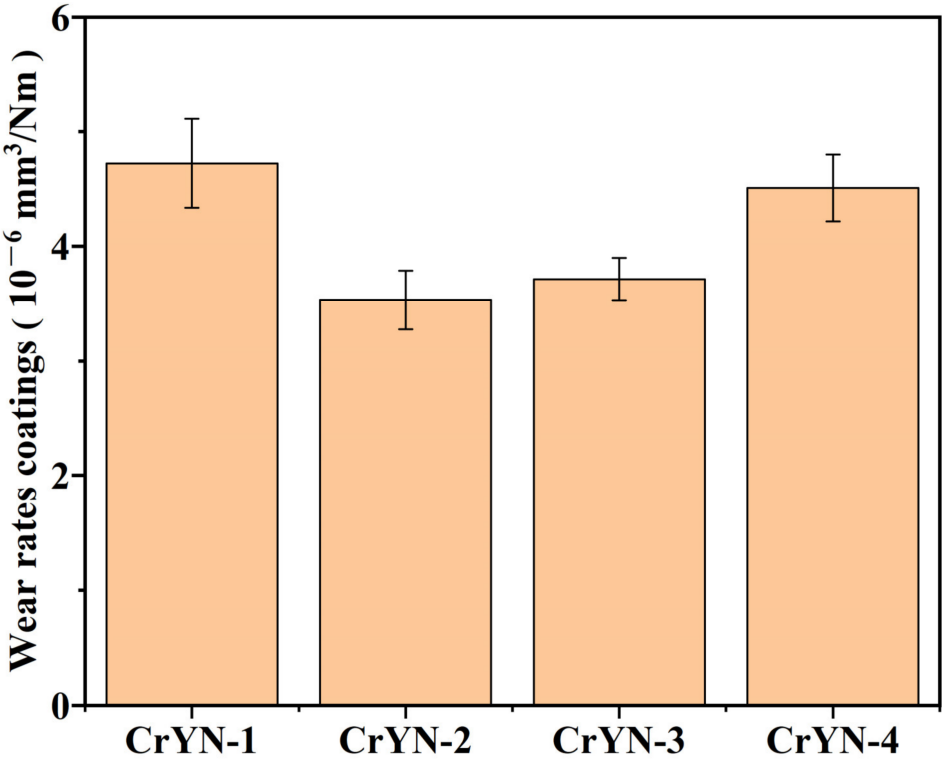

Figure 10. Wear rates of CrYN coatings of GCr15 balls in artificial seawater under various substrate bias voltages.

4. Conclusions

CrYN coatings were prepared using multi-arc ion plating at various substrate bias voltages (−50 V, −100 V, −150 V, and −200 V). X-ray diffractometry and scanning electron microscopy were used to characterize the composition and microstructure of the coatings. An electrochemical workstation and a ball-on-disk tribometer were used to investigate their corrosion and friction behavior. In this study, the following conclusions could be obtained.

(1) As the substrate bias voltage increased, the CrN (111), (200), and (220) peak intensities decreased and increased in width at half height;
(2) With increasing bias voltage, using yttrium (Y) in an amorphous form as a dopant restrained the grain growth, refined the grains, and improved the coating quality; moreover, the microhardness increased from 1985 hv to 2192 HV. The surfaces of the CrYN coatings prepared under bias voltages of −100 V and −150 V were smoother and more compact than those of the CrYN coatings prepared under bias voltages of −50 V and −200 V, corresponding to Y contents of 2.83 at.% and 3.1 at.%;
(3) The corrosion resistance of the coatings was mainly related to their surface, compactness, and material components. Electrochemical tests showed that the CrYN coatings deposited at a bias voltage of −100 V had the largest impedance values, the highest corrosion potentials, low self-corrosion currents, and good levels of resistance to electrolytic attack;
(4) In an artificial seawater friction test, the friction coefficients of deposited CrYN coatings under −100 V and −150 V bias voltages were all below 0.2, and the wear rates

were low. This was mainly because of their dense coating structure and good corrosion resistance. The wear mechanism of CrYN coatings in artificial seawater was shown to be a mix of tribochemical wear and adhesive wear.

Author Contributions: Conceptualization, M.L.; Methodology, M.L.; Investigation, Y.Y.; Resources, Z.W.; Data curation, Y.X.; Writing—original draft, M.L.; Writing—review and editing, M.L.; Project administration, C.T.; Funding acquisition, C.Z. and M.L. All authors have read and agreed to the published version of the manuscript.

Funding: This work was supported by Innovation team project of Guangdong Universities (2020KCXTD032), Natural Science Foundation of Guangdong Province (2021A1515011928, 2022A1515011137), and Zhanjiang science and technology project (2021B01512).

Data Availability Statement: Not applicable.

Conflicts of Interest: The authors declare that they have no known competing financial interest or personal relationships that could have influenced the work reported in this paper.

References

1. Wang, J.; Yan, F.; Xue, Q. Friction and Wear Behavior of Ultra-High Molecular Weight Polyethylene Sliding Against GCr15 Steel and Electroless Ni–P Alloy Coating Under the Lubrication of Seawater. *Tribol. Lett.* **2009**, *35*, 85–95. [CrossRef]
2. Cicek, V. Corrosion and Corrosion Prevention of Metallic Structures in Seawater. In *Corrosion Engineering and Cathodic Protection Handbook.*; John Wiley & Sons.: Milton, Australia, 2017; pp. 305–308.
3. Machuca, L.L.; Murray, L.; Gubner, R.; Bailey, S.I. Evaluation of the effects of seawater ingress into 316L lined pipes on corrosion performance. *Mater. Corros.* **2014**, *65*, 8–17. [CrossRef]
4. Du, C.; Bai, X.; Yuan, C. Fretting Tribocorrosion Behaviors of Marine Mooring Chain Steel 22MnCrNiMo in Artificial Seawater. *J. Tribol.* **2021**, *143*, 071701. [CrossRef]
5. Ye, Y.; Liu, Z.; Liu, W.; Zhang, D.; Wang, Y.; Zhao, H.; Li, X. Effect of interlayer design on friction and wear behaviors of CrAlSiN coating under high load in seawater. *RSC Adv.* **2018**, *8*, 5596–5607. [CrossRef] [PubMed]
6. Alkan, S.; Gök, M.S. Influence of plasma nitriding pre-treatment on the corrosion and tribocorrosion behaviours of PVD CrN, TiN and AlTiN coated AISI4140 steel in seawater. *Lubr. Sci.* **2021**, *34*, 67–83. [CrossRef]
7. Zhang, J.; Li, Z.; Wang, Y.; Zhou, S.; Wang, Y.; Zeng, Z.; Li, J. A new method to improve the tribological performance of metal nitride coating: A case study for CrN coating. *Vacuum* **2020**, *173*, 109158.
8. Wu, Z.; Zhou, F.; Ma, Q.; Wang, Q.; Zhou, Z.; Kwok-Yan Li, L. Tribological and electrochemical properties of Cr–Si–C–N coatings in artificial seawater. *RSC Adv.* **2016**, *6*, 76724–76735. [CrossRef]
9. Cai, F.; Yang, Q.; Huang, X. The Roles of Diffusion Factors in Electrochemical Corrosion of TiN and CrN (CrSiCN) Coated Mild Steel and Stainless Steel. In *Supplemental Proceedings: Volume 1: Materials Processing and Interfaces*; TMS: Pittsburgh, PA, USA, 2012; pp. 49–56.
10. Bernal, J.L.; Irvin, A.; Vera, E.; Olvera, P.N.; Villanueva, M.; Lasorsa, C.A.; Medina, A.; Bejar, L.; BorJas, S. Microstructural Characterization of Hardened AISI 4140 using CrN/CSi Coatings. *Microsc. Microanal.* **2017**, *23*, 416–417. [CrossRef]
11. Baseri, N.A.; Mohammadi, M.; Ghatee, M.; Abassi-Firouzjah, M.; Elmkhah, H. The effect of duty cycle on the mechanical and electrochemical corrosion properties of multilayer CrN/CrAlN coatings produced by cathodic arc evaporation. *Surf. Eng.* **2020**, *37*, 253–262. [CrossRef]
12. Filippov, A.; Vorontsov, A.; Shamarin, N.; Moskvichev, E.; Novitskaya, O.; Knyazhev, E.; Denisova, Y.; Leonov, A.; Denisov, V.; Tarasov, S. Dry Sliding Friction Study of ZrN/CrN Multi-Layer Coatings Characterized by Vibration and Acoustic Emission Signals. *Metals* **2022**, *12*, 2046. [CrossRef]
13. Iram, S.; Wang, J.; Cai, F.; Zhang, J.; Ahmad, F.; Liang, J.; Zhang, S. Effect of bilayer number on mechanical and wear behaviours of the AlCrN/AlCrMoN coatings by AIP method. *Surf. Eng.* **2020**, *37*, 536–544. [CrossRef]
14. Kim, G.S.; Kim, S.M.; Lee, S.Y.; Lee, B.Y. Comparative studies on the thermal stability and corrosion resistance of CrN, CrSiN, and CrSiN/AlN coatings. *J. Vac. Sci. Technol. A: Vac. Surf. Film.* **2009**, *27*, 873–879. [CrossRef]
15. Konchady, M.S.; Yarmolenko, S.; Pai, D.M.; Sankar, J. In Nanoindentation, Nanoscratch and Wear Studies on Nanoscale Multilayer TiN/CrN Coatings. In Proceedings of the ASME 2009 International Mechanical Engineering Congress and Exposition, Lake Buena Vista, FL, USA, 13–19 November 2009; pp. 55–59.
16. Luo, P.; Gong, C.; Li, Y.; Wang, X.; Tian, X. Effect of Auxiliary Enhanced Magnetic Field on Microstructure and Mechanical Behaviors of Multilayered CrN/AlCrN Films. *J. Mater. Eng. Perform.* **2021**, *31*, 230–239. [CrossRef]
17. Mundotia, R.; Thorat, N.J.; Kale, A.; Mhatre, U.; Kothari, D.C.; Kovacs, T.; Ghorude, T. Study of corrosion properties of CrN and multilayer CrN/Cr coating at different electrolyte temperatures deposited on stainless steel by vacuum arc process. *Dae Solid State Phys. Symp.* **2019**, *2115*, 030313.
18. Ren, Y.J.; Wen, W.; Chen, J.; Chen, J.L.; Qiu, W.; He, J.J. Corrosion behaviour of nanochromium coatings deposited by direct current magnetron sputtering. *Surf. Eng.* **2016**, *32*, 294–298. [CrossRef]

19. Wu, Z.; Cheng, Z.; Zhang, H.; Xu, Z.; Wang, Y.; Zhou, F. Electrochemical and Tribological Properties of CrAlN, TiAlN, and CrTiN Coatings in Water-Based Cutting Fluid. *J. Mater. Eng. Perform.* **2020**, *29*, 2153–2163. [CrossRef]
20. Aissani, L.; Fellah, M.; Nouveau, C.; Abdul Samad, M.; Montagne, A.; Iost, A. Structural and mechanical properties of Cr–Zr–N coatings with different Zr content. *Surf. Eng.* **2017**, *36*, 69–77. [CrossRef]
21. Selvam, L.; Murugesan, P.K.; Mani, D.; Natarajan, Y. Investigation of AlCrN-Coated Inserts on Cryogenic Turning of Ti-6Al-4V Alloy. *Metals* **2019**, *9*, 1338. [CrossRef]
22. Liu, S.; Ong, B.D.; Guo, J.; Liu, E.; Zeng, X. Wear performance of Y-doped nanolayered CrN/AlN coatings. *Surf. Coat. Technol.* **2019**, *367*, 349–357. [CrossRef]
23. Tritremmel, C.; Daniel, R.; Mitterer, C.; Mayrhofer, P.H.; Lechthaler, M.; Polcik, P. Oxidation behavior of arc evaporated Al-Cr-Si-N thin films. *J. Vac. Sci. Technol. A Vac. Surf. Film.* **2012**, *30*, 061501. [CrossRef]
24. Liu, S.; Wheeler, J.M.; Davis, C.E.; Clegg, W.J.; Zeng, X.T. The effect of Si content on the fracture toughness of CrAlN/Si3N4 coatings. *J. Appl. Phys.* **2016**, *119*, 025305.
25. Correa, J.F.; Caicedo, J.C.; Aperador, W.A. Comparison of Structural and Electrochemical Properties among TiCN, BCN, and CrAlN Coatings under Aggressive Environments. *J. Mater. Eng. Perform.* **2021**, *30*, 3586–3602.
26. Zhang, P.; Shan, L.; Tian, Y.; Su, X.; Luo, L.; Chen, J. Structure and tribological behavior of CrAlCN coating in artificial seawater. *Surf. Topogr. Metrol. Prop.* **2021**, *9*, 035028.
27. Radu, I.; Li, D.Y.; Llewellyn, R. Tribological behavior of Stellite 21 modified with yttrium. *Wear* **2004**, *257*, 1154–1166. [CrossRef]
28. Wu, Z.T.; Qi, Z.B.; Zhu, F.P.; Liu, B.; Wang, Z.C. Influences of Y Addition on Mechanical Properties and Oxidation Resistance of CrN Coating. *Phys. Procedia* **2013**, *50*, 150–155.
29. Rovere, F.; Mayrhofer, P.H. Impact of yttrium on structure and mechanical properties of Cr–Al–N thin films. *J. Vac. Sci. Technol. A: Vac. Surf. Film.* **2007**, *25*, 1336–1440. [CrossRef]
30. Wang, Y.-X.; Wu, S.-L.; Pan, J.; Zhang, X. Effect of Y content on the microstructure, tribological and corrosion properties of CrAlYN coatings deposited by magnetron sputtering. *Mater. Res. Express* **2019**, *6*, 096402. [CrossRef]
31. ASTM D1141-98. Standard Practice for Preparation of Substitute Ocean Water. ASTM: West Conshohocken, PA, USA, 2021.
32. ASTM G102-89e1. Standard Practice for Calculation of Corrosion Rates and Related Information from Electrochemi cal Measurements. ASTM: West Conshohocken, PA, USA, 2015.
33. Shiao, M.H.; Chang, Z.C.; Shieu, F.S. Characterization and Formation Mechanism of Macroparticles in Arc Ion-Plated CrN Thin Films. *J. Electrochem. Soc.* **2003**, *150*, C320.
34. Goto, H.; Akao, N.; Hara, N.; Sugimoto, K. Pinhole Defect Density of CrNx Thin Films Formed by Ion-Beam-Enhanced Deposition on Stainless Steel Substrates. *J. Electrochem. Soc.* **2007**, *154*, C189.
35. Rovere, F.; Mayrhofer, P.H.; Reinholdt, A.; Mayer, J.; Schneider, J.M. The effect of yttrium incorporation on the oxidation resistance of Cr–Al–N coatings. *Surf. Coat. Technol.* **2008**, *202*, 5870–5875. [CrossRef]
36. Chunyan, Y.; Linhai, T.; Yinghui, W.; Shebin, W.; Tianbao, L.; Bingshe, X. The effect of substrate bias voltages on impact resistance of CrAlN coatings deposited by modified ion beam enhanced magnetron sputtering. *Appl. Surf. Sci.* **2009**, *255*, 4033–4038. [CrossRef]
37. Tlili, B.; Mustapha, N.; Nouveau, C.; Benlatreche, Y.; Guillemot, G.; Lambertin, M. Correlation between thermal properties and aluminum fractions in CrAlN layers deposited by PVD technique. *Vacuum* **2010**, *84*, 1067–1074. [CrossRef]
38. Tjong, S.C.; Chen, H. Nanocrystalline materials and coatings. *Mater. Sci. Eng. R: Rep.* **2004**, *45*, 1–88. [CrossRef]
39. Wan, X.S.; Zhao, S.S.; Yang, Y.; Gong, J.; Sun, C. Effects of nitrogen pressure and pulse bias voltage on the properties of CrN coatings deposited by arc ion plating. *Surf. Coat. Technol.* **2010**, *204*, 1800–1810. [CrossRef]
40. Warcholinski, B.; Gilewicz, A.; Ratajski, J.; Kuklinski, Z.; Rochowicz, J. An analysis of macroparticle-related defects on CrCN and CrN coatings in dependence of the substrate bias voltage. *Vacuum* **2012**, *86*, 1235–1239.
41. Romero, J.; Gómez, M.A.; Esteve, J.; Montalà, F.; Carreras, L.; Grifol, M.; Lousa, A. CrAlN coatings deposited by cathodic arc evaporation at different substrate bias. *Thin Solid Film.* **2006**, *515*, 113–117. [CrossRef]
42. Liu, C.; Bi, Q.; Leyland, A.; Matthews, A. An electrochemical impedance spectroscopy study of the corrosion behaviour of PVD coated steels in 0.5 N NaCl aqueous solution: Part II.: EIS interpretation of corrosion behaviour. *Corros. Sci.* **2003**, *45*, 1257–1273. [CrossRef]
43. Abd El-Rahman, A.M.; Wei, R. Effect of ion bombardment on structural, mechanical, erosion and corrosion properties of Ti–Si–C–N nanocomposite coatings. *Surf. Coat. Technol.* **2014**, *258*, 320–328.
44. Barshilia, H.C.; Prakash, M.S.; Poojari, A.; Rajam, K.S. Corrosion Behaviour of TiN/a-C Superhard Nanocomposite Coatings Prepared by a Reactive DC Magnetron Sputtering Process. *Trans. IMF* **2017**, *82*, 123–128. [CrossRef]
45. Dong, M.; Zhu, Y.; Xu, L.; Ren, X.; Ma, F.; Mao, F.; Wang, L. Tribocorrosion performance of nano-layered coating in artificial seawater. *Appl. Surf. Sci.* **2019**, *487*, 647–654. [CrossRef]
46. Shan, L.; Wang, Y.; Li, J.; Li, H.; Wu, X.; Chen, J. Tribological behaviours of PVD TiN and TiCN coatings in artificial seawater. *Surf. Coat. Technol.* **2013**, *226*, 40–50. [CrossRef]

47. Ye, Y.; Wang, Y.; Chen, H.; Li, J.; Zhou, S.; Xue, Q. Influences of bias voltage on the microstructures and tribological performances of CrCN coatings in seawater. *Surf. Coat. Technol.* **2015**, *270*, 305–313. [CrossRef]
48. Chen, B.; Wang, J.; Yan, F. Friction and Wear Behaviors of Several Polymers Sliding Against GCr15 and 316 Steel Under the Lubrication of Sea Water. *Tribol. Lett.* **2011**, *42*, 17–25. [CrossRef]